J|A|C|S
ARTICLES
Published on Web 06/28/2006

Spinel-to-$CaFe_2O_4$-Type Structural Transformation in $LiMn_2O_4$ under High Pressure

Kazunari Yamaura,*,† Qingzhen Huang,‡ Lianqi Zhang,§ Kazunori Takada,§ Yuji Baba,|| Takuro Nagai,|| Yoshio Matsui,|| Kosuke Kosuda,⊥ and Eiji Takayama-Muromachi†

Contribution from the Advanced Nano Materials Laboratory, National Institute for Materials Science, 1-1 Namiki, Tsukuba, Ibaraki 305-0044, Japan, NIST Center for Neutron Research, National Institute of Standards and Technology, Gaithersburg, Maryland 20899, Nanoscale Materials Center, National Institute for Materials Science, 1-1 Namiki, Tsukuba, Ibaraki 305-0044, Japan, Advanced Nano Characterization Center, National Institute for Materials Science, 1-1 Namiki, Tsukuba, Ibaraki 305-0044, Japan, and Materials Analysis Station, National Institute for Materials Science, 1-1 Namiki, Tsukuba, Ibaraki 305-0044, Japan

Received February 21, 2006; E-mail: YAMAURA.Kazunari@nims.go.jp

Abstract: A new form of $LiMn_2O_4$ is reported. The structure is the $CaFe_2O_4$-type and 6% denser than the spinel. The structure transformation was achieved by heating at 6 GPa. Analysis of the neutron diffraction pattern confirmed an average of the structure; the unit cell was orthorhombic at $a = 8.8336(5)$ Å, $b = 2.83387(18)$ Å, and $c = 10.6535(7)$ Å (*Pnma*). Electron diffraction patterns indicated an order of superstructure $3a \times b \times c$, which might be initiated by Li vacancies. The exact composition is estimated at $Li_{0.92}Mn_2O_4$ from the structure analysis and quantity of intercalated Li. The polycrystalline $CaFe_2O_4$-type compound showed semiconducting-like characters over the studied range above 5 K. The activation energy was reduced to ~0.27 eV from ~0.40 eV at the spinel form, suggesting a possible enhancement of hopping mobility. Magnetic and specific-heat data indicated a magnetically glassy transition at ~10 K. As the $CaFe_2O_4$-type transition was observed for the mineral $MgAl_2O_4$, hence the new form of the lithium manganese oxide would provide valuable opportunities to study not only the magnetism of strongly correlated electrons but also the thermodynamics of the phase transition in the mantle.

Introduction

$LiMn_2O_4$ spinel is a geometrically frustrated antiferromagnetic material. Recent research progress indicates that the magnetic property is accompanied by a degree of charge segregation.[1−5] The association might result in the complicated magnetic ground state: neutron scattering detected substantial diffuse reflections remaining far below the magnetic transition temperature ~60 K,[5] while neutron polarization analysis revealed nearly half of spins are ordered.[1] The magnetic properties are highly sensitive to the material stoichiometry probably due to the relation to the charge segregation:[2] the magnetic nature is indeed profoundly influenced by the electrochemical method.[3] Due to the rather complicated magnetic properties further investigations including magnetic and structural studies would be required to establish a solid picture of the unusual magnetic state.

Here we report the discovery of a structure transformation in the compound. The spinel structure was found transforming to another under high pressure, 6GPa, during heating at 1100 °C or above. The high-pressure (HP) form was identified as the $CaFe_2O_4$ (calcium ferrite)-type,[6−8] which is approximately 6% more dense than the spinel. As one of the key materials of geological science, "Spinel" $MgAl_2O_4$ shows the calcium ferrite-type transition;[9−11] hence it would be of value to study the structure thermodynamics in $LiMn_2O_4$, because the transition appears in a rather moderate pressure range than in the mantle. Very recently, $CuRh_2O_4$ was found to show a corresponding structure transition under high pressure.[12]

In the calcium ferrite-type structure, all manganese ions are in a 6-fold coordinated environment by oxygen as well as in the perovskite manganese oxides, which show a broad range

† ANML, National Institute for Materials Science.
‡ National Institute of Standards and Technology.
§ NMC, National Institute for Materials Science.
|| ANCC, National Institute for Materials Science.
⊥ MAS, National Institute for Materials Science.

(1) Greedan, J. E.; Wiebe, C. R.; Wills, A. S.; Stewart, J. R. *Phys. Rev. B* **2002**, *65*, 184424.
(2) Tachibana, M.; Tojo, T.; Kawaji, H.; Atake, T.; Yonemura, M.; Kanno, R. *Phys. Rev. B* **2002**, *65*, 184424.
(3) Jang, Y.; Huang, B.; Chou, F. C.; Sadoway, D. R.; Chiang, Y. M. *J. Appl. Phys.* **2000**, *87*, 7382.
(4) Greedan, J. E. *J. Mater. Chem.* **2001**, *11*, 37.
(5) Wills, A. S.; Raju, N. P.; Greedan, J. E. *Chem. Mater.* **1999**, *11*, 1510.
(6) Akimoto, J.; Awaka, J.; Kijima, N.; Takahashi, Y.; Maruta, Y.; Tokiwa, K.; Watanabe, T. *J. Solid State Chem.* **2005**, *178*, 3929.
(7) Regan, K. A.; Huang, Q.; Lee, M.; Ramirez, A. P.; Cava, R. J. *J. Solid State Chem.* **2005**, *179*, 193.
(8) Yamaura, K.; Huang, Q.; Moldovan, M.; Young, D. P.; Sato, A.; Baba, Y.; Nagai, T.; Matsui, Y.; Takayama-Muromachi, E. *Chem. Mater.* **2005**, *17*, 359.
(9) Irifune, T.; Naka, H.; Sanehira, T.; Inoue, T.; Funakoshi, K. *Phys. Chem. Miner.* **2002**, *29*, 645.
(10) Catti, M. *Phys. Chem. Miner.* **2001**, *8*, 729.
(11) Irifune, T.; Fujino, K.; Ohtani, E. *Nature* **1991**, *349*, 409.
(12) Ohgushi, K.; Gotou, H.; Yagi, T.; Ueda, Y. *J. Phys. Soc. Jpn.* **2006**, *75*, 023707.

10.1021/ja0612302 CCC: $33.50

of magnetic and electrical properties.[13] Furthermore, the MnO_6 forms a double chain-type unit, in which magnetic anisotropy is inherent. We then expect the new form of $LiMn_2O_4$ would be valuable also for studies to expand understanding of the correlated electron nature of the perovskite manganese oxides.

In this study, the structure transformation was investigated by neutron, X-ray, and electron diffraction, and the magnetic properties of the new form of $LiMn_2O_4$ are reported.

Experimental Section

Sample Preparation. Polycrystalline spinel $LiMn_2O_4$ was prepared from fine powders Li_2CO_3 (4N) and Mn_2O_3 (4N). The Mn_2O_3 powder was preheated in air at 650 °C for 18 h. To test an effect of possible Li volatility on the sample quality, stoichiometric (Li/Mn = 1/2) and 6% Li-excess (1.06/2) mixtures were heated simultaneously. At first, those were heated in air at 700 °C for 18 h in an alumina crucible with a cap, followed by cooling and grinding. The heating was then repeated at 800 °C for 12 h and then at 850 °C for 60 h. The products were examined by powder X-ray diffraction method (Cu Kα, RIGAKU RINT2000), and we confirmed both samples were of high quality and qualitatively equivalent. More specifically, the cubic lattice constant was $a = 8.251(1)$ Å and 8.252(1) Å for the Li/Mn = 1/2 and 1.06/2 samples, respectively, which are in good accord with what was reported elsewhere.[14] The X-ray result suggested both samples were nearly stoichiometric, regardless of the nominal composition.

The spinel powder prepared at the Li/Mn = 1/2 composition was employed for the next round of synthesis. The powder was placed in a gold capsule, and the capsule was installed in a high-pressure apparatus that is capable of maintaining 6 GPa during heating. The elevated temperature was 900 °C, 1000 °C, 1100 °C, 1200 °C, and 1500 °C for each run, and the heating duration was fixed at 1 h. A platinum capsule was used for the 1500 °C synthesis, because it should be above the melting point of gold.[15] After the heating, the capsule was quenched in the high-pressure apparatus before releasing the pressure. The Mn_2O_3 and $KClO_4$ powders were used with the spinel powder to prepare Li-reduced samples in the same manner.

All HP products were examined by the X-ray powder diffraction method, and the best quality sample (prepared at 1500 °C) was subjected for an electron probe microanalysis [EPMA] (JEOL, JXA-8500F). The acceleration voltage was 15.0 kV. The surface of the selected sample was polished carefully on a fine alumina (~0.3 μm) coated film before the EPMA. As a result, no contribution from the platinum capsule was detected above the background level, and the KCl residue was confirmed as expected. The quantitative data were categorized into two groups; the composition of the major group was O/Mn = 1.95(3) and 2.85(3) for the other. A scanning electron image was taken at a magnitude of 1×10^4 in EPMA.

Structure Analysis. The same sample was reemployed for the neutron diffraction study. The sample powder was rinsed in water to remove the KCl residue and dried in nitrogen gas without heating. The sample mass was 4.8 g. The powder was set in the BT-1 high-resolution diffractometer at the NIST Center for Neutron Research, employing a Cu(311) monochromator. Collimators with horizontal divergences of 15′, 20′, and 7′ of arc were used before and after the monochromator and after the sample, respectively. The calibrated neutron wavelength was $\lambda = 0.154\,03$ nm, and drift was negligible during the data collection. A detailed description of the facility is available online.[16] The intensity of neutron reflection was measured at every 0.05° step over the 2θ range from 3° to 168°. The sample was hold at room temperature during the measurement. Neutron scattering amplitudes used in the data refinements were 0.190, 0.375, and 0.581 ($\times 10^{-12}$ cm) for Li, Mn, and O, respectively.

A part of the sample was studied by electron diffraction (ED) on a Hitachi H-1500 electron microscope, in which the electrons were accelerated at 820 kV.

Physical Property Measurements. Parts of the sample were subjected for electrical and magnetic measurements. The sample pellet as made in the high-pressure furnace was cut into a bar shape and wired for the four-terminal resistivity measurement. The study was conducted between 5 K and 390 K in a commercial apparatus (Quantum design, PPMS). The ac-gage current was 0.1 mA, and the ac-frequency was 30 Hz. The specific heat of the sample was measured in the PPMS apparatus by a time-relaxation method between 1.8 K and 60 K.

Magnetic susceptibility was measured in magnetic fields of 50 Oe and 70 kOe. The sample was cooled to 1.8 K without the field, and then the magnetic field was applied, followed by heating to 350 K (zero-field cooling, ZFC) and cooling again to 1.8 K (field-cooling, FC) in a commercial apparatus (Quantum design, MPMS). The magnetization study was conducted in the apparatus at 2 K, 20 K, 30 K, and 50 K within the field range ±70 kOe.

Lithium Intercalation. Li ions were intercalated into the sample in a two-electrode electrochemical cell between 1.0 V and 4.5 V. The working electrode consisted of the sample (20 mg) and conductive binder (8 mg of poly(tetrafluoroethylene) and 4 mg of acetylene black), which was pressed on a titanium mesh at 300 kg/cm^2 and then dried in argon at room temperature for 48 h. A lithium foil was used as the counter electrode. The electrolyte solution was a mixture of ethylene carbonate and diethyl carbonate with a volume ratio of 1/1 containing 1 M $LiPF_6$ as a supporting salt. The cathodic current was 20 mA/g (0.22 mA/cm^2).

Results and Discussion

X-ray powder diffraction patterns for the samples prepared under the high-pressure condition are shown in Figure 1. For easy comparison the pattern of the starting spinel is shown as well. Each number at the left side indicates the heating temperature. The patterns clearly indicate a formation of another structure under the synthesis conditions at 1100 °C or above. To identify the structure, several structure models were tested on the peak distribution, and we found the $CaFe_2O_4$-type was most likely. The peak positions were well characterized by assuming the $CaFe_2O_4$-type orthorhombic unit cell with lattice constants $a = 8.836(1)$ Å, $b = 2.834(1)$ Å, and $c = 10.65(1)$ Å (*Pnma* for the 1100 °C profile). The compound is probably isostructural with $NaRh_2O_4$, $NaRu_2O_4$, and $NaMn_2O_4$, which were recently studied,[6−8] and the results thus suggest the spinel-type $LiMn_2O_4$ goes into the $CaFe_2O_4$-type under the high-pressure condition. To confirm the transformation, we considered a neutron diffraction study, as the X-ray patterns may have limited information about oxygen and lithium. We then tried to improve the sample quality by optimizing the synthesis conditions in order to gain reliability of the neutron structure analysis.

The samples heated at 1100 °C or above were found to contain a small amount of impurity as marked by stars "*" in Figure 1. The impurity was identified as Li_2MnO_3[17,18] from the X-ray pattern and the EPMA result. The presence of the impurity in the final product suggests that Li deficiency in the main compound might be a possible Li source of the impurity. To get rid of the possible Li source, a Li-reduced mixture (nominal

(13) Imada, M.; Fujimori, A.; Tokura Y. *Rev. Mod. Phys.* **1998**, *70*, 1039.
(14) Akimoto, J.; Takahashi, Y.; Gotoh, Y.; Mizuta, S. *Chem. Mater.* **2000**, *12*, 3246.
(15) Mirwald, P. W.; Getting, I. C.; Kennedy, G. C. *J. Geophys. Res.* **1975**, *80*, 1519.
(16) http://www.ncnr.nist.gov/programs/crystallography/.
(17) Riou, A.; Lecerf, A.; Gerault, Y.; Cudennec, Y. *Mater. Res. Bull.* **1992**, *27*, 269.
(18) Strobel, P.; Lambert-Andron, B. *J. Solid State Chem.* **1988**, *75*, 90.

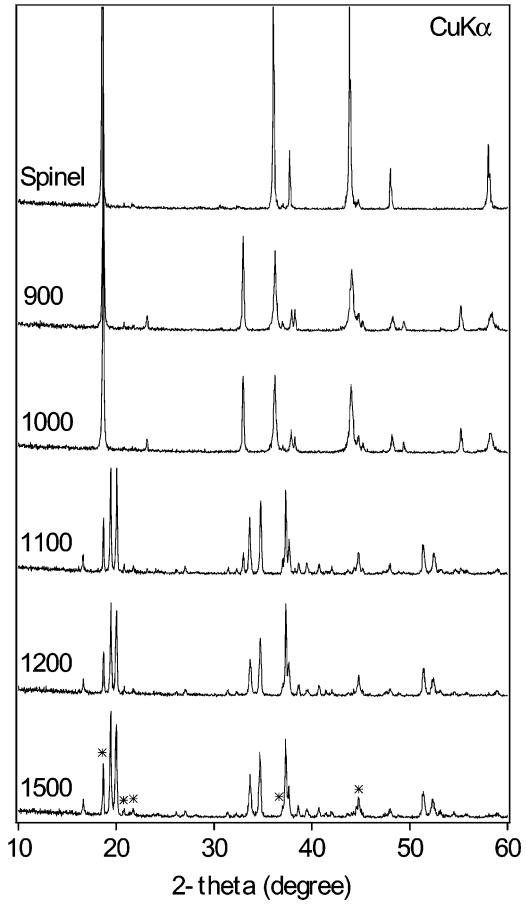

Figure 1. X-ray diffraction profiles of the lithium manganese oxides before (top) and after the high-pressure heating. The number of each pattern indicates heating temperature (°C) at 6 GPa. Asterisks (*) indicate the Li_2MnO_3 peaks.

composition was Li/Mn = 0.9/2, if the starting powders are stoichiometric) was heated at 6 GPa and 1500 °C for 1 h in the same synthesis manner, and we found that the amount of Li_2MnO_3 was indeed reduced in the final product. Many Li-reduced mixtures (Li/Mn = 0.8/2, 0.75/2, and 0.5/2) were also tested. However, the product quality was poor; other impurities appeared, unfortunately.

Apart form the consideration about the possible Li deficiency, other various nominal compositions, including Li excess (the maximum Li content was 1.2 mol per the formula unit) and oxygen excess (the maximum oxygen content was 4.2 per the formula unit), were tested over the heating range between 1100 °C and 1500 °C at 6 GPa. However, no indications of sample quality improvement were seen, and then we decided to take the sample at the Li/Mn = 0.9/2 composition for the neutron diffraction study.

We had another problem in the sample preparation. In each high-pressure run, approximately 0.8 g sample was produced, and we found it was too little for the neutron diffraction study. We therefore needed to repeat the synthesis run 8 times to increase the sample mass. All products were examined by the X-ray diffraction method, and all were found equivalent in quality. Six products were subjected to the neutron diffraction study, and the other two were reserved for the other chemical and magnetic studies. The X-ray diffraction pattern of the mixture of the six products is shown in Figure 2.

The neutron diffraction study was conducted in the NIST center for neutron research. The obtained pattern at room temperature was analyzed with the GSAS software.[19,20] The initial parameters were employed from the structure of $NaMn_2O_4$ (Space group: *Pnma*, $a = 8.9055(18)$ Å, $b = 2.8524(5)$ Å, and $c = 11.0825(22)$ Å).[6] Preliminary fits to the neutron diffraction pattern suggested it was much more reasonable than the other structure models, such as $CaMn_2O_4$ (Space group: *Pbcm*, $a = 3.1492(6)$ Å, $b = 9.98(2)$ Å, and $c = 9.66(2)$ Å)[21,22] and $CaTi_2O_4$ (Space group: *Bbmm*, $a = 9.718(4)$ Å, $b = 9.9960(4)$ Å, and $c = 3.140(2)$ Å).[23] Perhaps, if the largest and the next largest

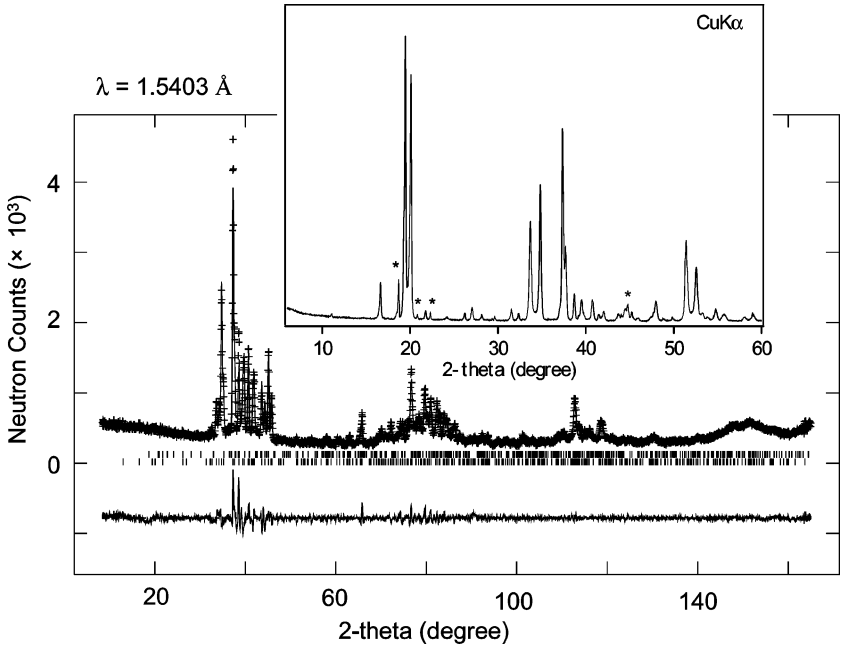

Figure 2. Powder neutron diffraction profile (main panel) and X-ray diffraction profile (small panel) of the selected sample. Observed (+) and calculated (solid lines) intensities and differences between those (bottom) are shown. Vertical small bars indicate reflection positions for Li_2MnO_3 (upper) and $Li_{0.92}Mn_2O_4$ (lower). Asterisks (*) indicate X-ray peaks for Li_2MnO_3. The sample was at room temperature.

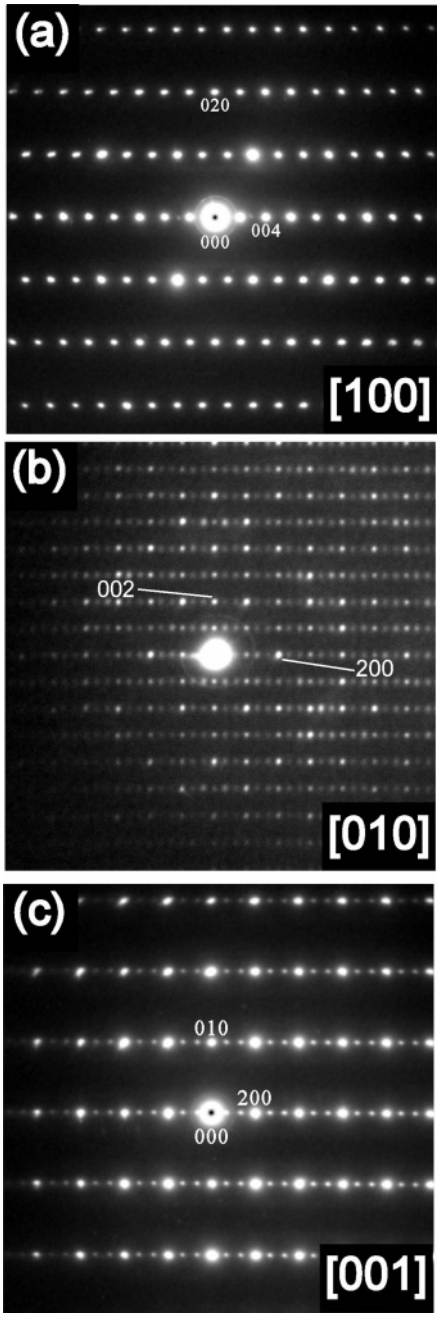

Figure 3. Electron diffraction patterns of the $CaFe_2O_4$-type $Li_{0.92}Mn_2O_4$ taken at room temperature. The zone axis was (a) [100], (b) [010], and (c) [001].

lattice constants are much closer, either the *Pbcm* or the *Bbmm* model might be more likely than the *Pnma* structure model of the compound.

To complete the structure analysis, we needed to investigate the probable Li deficiency. In the ED patterns, we found extra spots indicating a superstructure, which might be initiated by the Li vacancies. Representative patterns are shown in Figure 3a−c. Those clearly indicate not only the primary spots (the orthorhombic unit cell) but also small extra reflections along a^*. Neither a diffuse nor a sharp anomaly was seen in the other directions. The order of the superstructure is then concluded to be $3a \times b \times c$, where $a \times b \times c$ denotes the orthorhombic unit cell. The observed extinction order indicated the space group *Pnma* for the 3*a*-type superstructure as well as the average structure.

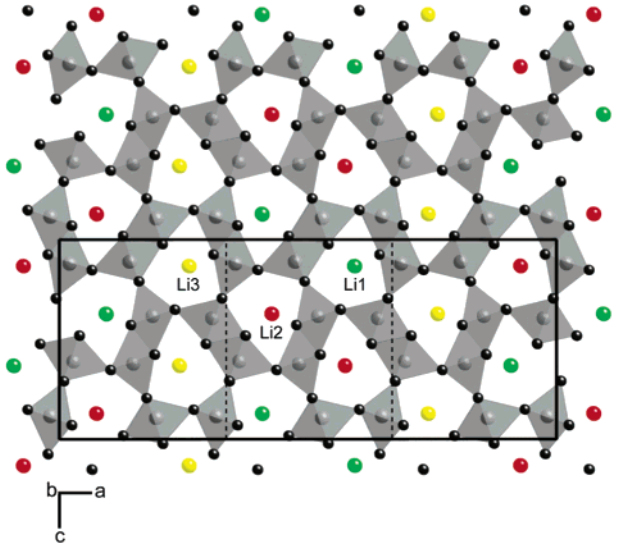

Figure 4. Sketch of the $3a \times b \times c$ superstructure model. Solid and dotted lines indicate the 3*a*-type and the average unit cell, respectively. One of three Li sites is assumed having a vacancy per the large unit cell.

More specifically, the (200) index in Figure 3c seems not to match with the other spots in Figure 3b. It was, however, confirmed, due to double diffraction, as the same order of spots that appeared during the sample analysis was tilted somewhat along the *a*-axis.[24,25] Additional ED patterns are available in the Supporting Information.

The 3*a*-type superstructure is probably due to ordering of Li vacancies and the local modification in the vicinity of the vacancy. In Figure 4, a sketch of the 3*a*-type superstructure model is shown. The solid lines indicate the $3a \times b \times c$ cell viewed from the *b*-axis direction, while the dotted lines indicate the average unit cell. In the superstructure model, we divided the Li site into Li1 to Li3 sites, where a quarter amount of Li in one of the three Li sites was absent, resulting in the Li composition 0.9167 [=(0.75+1+1)/3] per the formula. The electron diffraction simulation using the software named "MacTempas" suggested the vacancies are likely in either the Li1 or the Li2 site rather than the Li3 site within simulations with the parameters of accelerated voltage, 820 kV, the spherical aberration coefficient of an electron-optical objective lens, 2.2 mm, and the sample thickness,10 nm, 20 nm, and 30 nm. To gain further information about the 3*a*-type superstructure we conducted the Rietveld refinement on the neutron profile using both the average and the 3*a*-type models.

First, we tried the average structure model on the neutron profile. In the Rietveld analysis, the parameters for the minor phase Li_2MnO_3[17] were refined together with those for the main phase. In an early stage, the unfixed Li site occupancy factor

(19) Larson, A. C.; Von Dreele, R. B. *Los Alamos National Laboratory Report LAUR*; 2000; p 86.
(20) Toby, B. H. *J. Appl. Crystallogr.* **2001**, *34*, 210.
(21) Zouari, S.; Ranno, L.; Cheikh-Rouhou, A.; Isnard, O. Pernet, M.; Wolfers, P.; Strobel, P. *J. Alloys Compd.* **2003**, *353*, 5.
(22) Ling, C. D.; Neumeier, J. J.; Argyriou, D. N. *J. Solid State Chem.* **2001**, *160*, 167.
(23) Matthew, P. R.; Caldwell, J. H.; Ingram, D. R.; Green, C. E.; Geselbracht, M. J.; Siegrist, T. *J. Solid State Chem.* **1998**, *141*, 338.
(24) Asada, T.; Koyama, Y. *Phys. Rev. B* **2004**, *69*, 104108.
(25) Asaka T.; Nemoto, K.; Kimoto, K.; Arima, T.; Matsui Y. *Phys. Rev. B* **2005**, *71*, 014114.

Table 1. Atomic Coordinates and Isotropic Displacement Parameters of the Average Structure of $Li_{0.92}Mn_2O_4$ (HP)[a]

atom	*x*	*y*	*z*	$100U_{iso}$ (Å^2)	fraction
Li	0.278(4)	1/4	0.370(4)	12.7(14)	0.9167
Mn1	0.0584(10)	1/4	0.1188(8)	3.49(22)	1
Mn2	0.0828(8)	1/4	0.6082(6)	1.46(14)	1
O1	0.3061(6)	1/4	0.6508(6)	3.43(12)	1
O2	0.3801(9)	1/4	0.9799(6)	6.28(20)	1
O3	0.4764(8)	1/4	0.2072(6)	5.15(18)	1
O4	0.0707(8)	1/4	0.9269(6)	5.35(19)	1

[a] Space group: *Pnma*, $a = 8.8336(5)$ Å, $b = 2.83387(18)$ Å, $c = 10.6535(7)$ Å, $z = 4$, Cell volume $= 266.691(29)$ Å^3.

Table 2. Selected Bond Distances and Angles in the Average Structure of $Li_{0.92}Mn_2O_4$ (HP)

atoms		distances (Å)	atoms	angles (deg)
Li	O1 × 2	2.829(33)	Mn1−O1−Mn1	97.4(5)
	O2 × 2	2.313(30)	Mn1−O4−Mn1	103.1(4)
	O3	2.46(4)	Mn1−O4−Mn1	97.6(5)
	O3	2.79(4)	Mn1−O1−Mn2	125.3(3)
	O4 × 2	2.038(30)	Mn1−O3−Mn2	129.5(2)
Mn1	O1 × 2	1.886(7)	Mn1−O3−Mn2	129.5(2)
	O3	1.991(11)	Mn2−O2−Mn2	90.5(4)
	O4	2.047(10)	Mn2−O2−Mn2	100.0(4)
	O4 × 2	1.883(7)	Mn2−O3−Mn2	100.6(5)
Mn2	O1	2.025(9)		
	O2 × 2	1.995(7)		
	O2	2.021(11)		
	O3 × 2	1.842(6)		

was tested, and we found the solutions became unstable; thermal displacement factors of Mn1 and Mn2 fell into an unreasonably small level, below 0.1 Å^2 ($100U_{iso}$), and the Li occupancy factor slightly exceeded 1. This curious feature might imply a structure modulation such as the 3*a*-type superstructure. The Li-site occupancy was then fixed at 0.9167 ($=1 - 1/12$), as $1/12$ mol of Li per the formula unit were assumed absent (see the sketch in Figure 4). Shortly afterward, we could reach a much improved solution; the *R* factors wR_p and R_p were 6.68% and 5.13%, respectively. Alternative possibilities, such as mixing of Li and Mn, were tested, and no improvement was achieved.

The refinement result is shown in the main panel of Figure 2, the average structure parameters are listed in Tables 1 and 2, and the crystal structure is outlined from the solutions in Figure 5. The thermal displacement parameter of Li is remarkably large, probably due to the structure anomaly. While the data are valid within the average picture, however the result could be sufficient to confirm the transformation to the $CaFe_2O_4$-type from the spinel. The calculated density increases 6% by the transformation.

Next, the 3*a*-type superstructure model was considered to fit the neutron profile instead of the average model. The starting parameters were employed from Table 1, and the best results are shown in Figure 6a and Tables 3 and 4. As the fit quality was practically comparable (wR_p and R_p were 7.59 and 5.86, respectively) to those of the average analysis, a significant improvement was not achieved in this way. Although the $3a \times b \times c$ model is probably much closer to a true structure, however the present pattern quality might hinder the delicate refinement analysis over the larger unit cell. The X-ray diffraction pattern was also tested with the 3*a*-type cell (Figure 6b); however little progress in understanding the superstructure was attained. To reveal the nature of the superstructure, further sample quality improvement and advanced structure studies are needed. Preparing a high-quality single crystal is also alternative to the purpose.

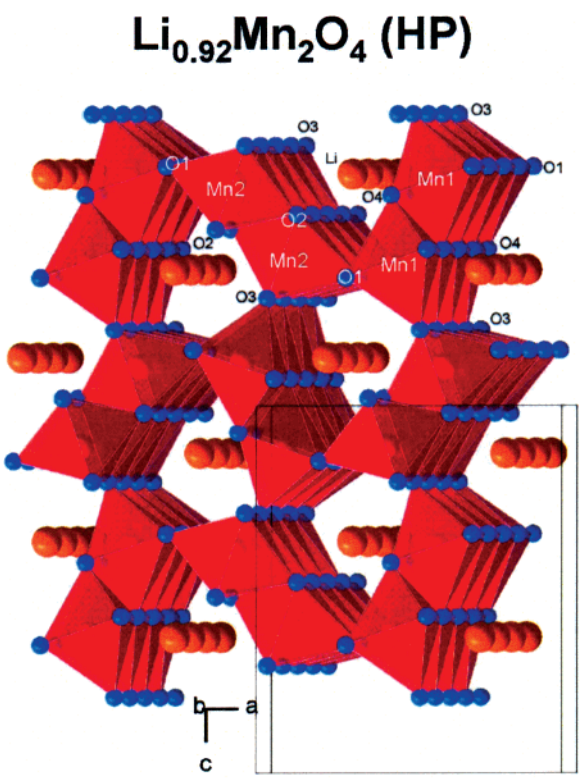

Figure 5. Average structure view of the $CaFe_2O_4$-type $Li_{0.92}Mn_2O_4$, based on the result of the neutron diffraction study. Solid lines indicate the orthorhombic unit cell.

The Rietveld analysis yielded the weight fraction of Li_2MnO_3, being 5.8(1)%. Hence, the total composition of the sample should be 1.15/2 (=Li/Mn, assuming the main phase composition is $Li_{0.92}Mn_2O_4$). The estimation does not match with the starting composition 0.9/2. Perhaps, other impurities might be involved somewhat in the sample, or a reaction with the platinum capsule at the surface of the pellet may complicate the sample composition, as often observed in high-pressure synthesis. A possibility of an additional amount of Li vacancies of the main phase was not excluded; we then conducted a quantitative measure of the Li vacancies by an electrochemical method.

In Figure 7, the potential data are shown: the potential decreases with the increasing amount of intercalated Li ions, *y* in $Li_{0.92+y}Mn_2O_4$, and then sharply dropped at $y = 0.08-0.09$, indicating the intercalation limit of the structure. The quantity matches well with the expectation from the 3*a*-type superstructure model. In addition, a scanning electron image of the sample is shown in Figure 8, in which the morphology and the size of particles are seen. The observation was intended to investigate possible factors, which might affect the intercalation; however, we did not see any of the possibilities.

Details of the local structure around the manganese ion is outlined in Figure 9 from the average structure data and compared with that of related compounds. The average bond distance to coordinated oxygen is 1.93(7) Å and 1.95(9) Å for Mn1 and Mn2, respectively, and a distortion factor of the Mn−O octahedra (defined as the ratio of the longest to the shortest bond distance) is 8.7% and 9.9% for $Mn1-O_6$ and $Mn2-O_6$, respectively. The result seems intermediate between that of the spinel $LiMn_2O_4$, in which no distortion was reported,[14] and that of $NaMn_2O_4$, in which a significant distortion 17% ($Mn1-O_6$) was found.[6] Although a small distortion was detected, the local

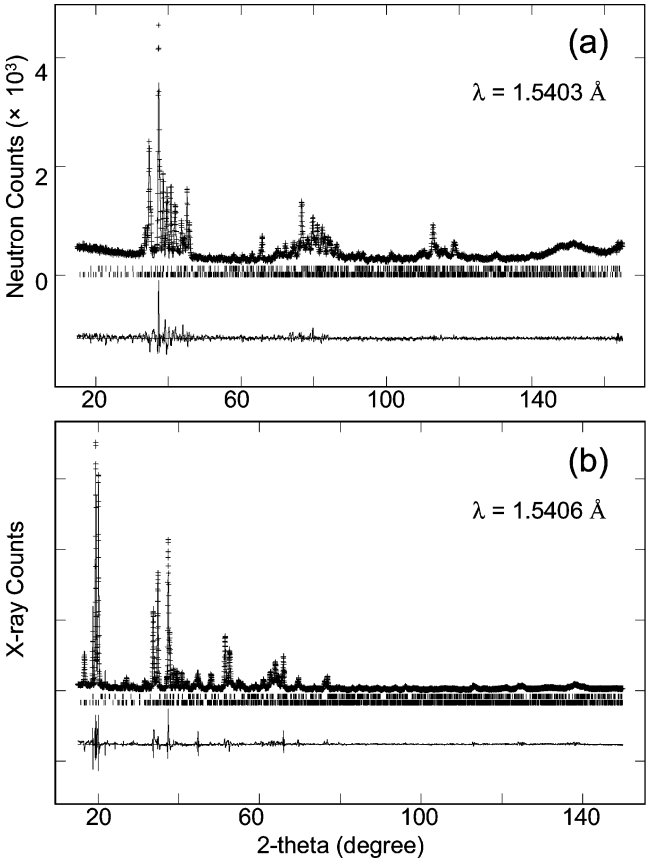

Figure 6. Rietveld study on (a) the neutron and (b) the X-ray diffraction patterns using the 3*a*-type superstructure model.

Table 3. Atomic Coordinates and Isotropic Displacement Parameters of the 3*a*-Type Superstructure of $Li_{0.92}Mn_2O_4$ (HP)[a]

atom	*x*	*y*	*z*	$100U_{iso}$ (Å^2)	fraction
Li1	0.0852(11)	1/4	0.3461(39)	3.491(14)	0.75
Li2	0.4175(9)	1/4	0.3407(28)	3.491(14)	1
Li3	0.7384(10)	1/4	0.3881(22)	3.491(14)	1
Mn11	0.0191(5)	1/4	0.1144(13)	3.491(14)	1
Mn12	0.3388(5)	1/4	0.1173(11)	3.491(14)	1
Mn13	0.6880(5)	1/4	0.1146(13)	3.491(14)	1
Mn21	0.0311(5)	1/4	0.6030(10)	3.491(14)	1
Mn22	0.3630(5)	1/4	0.6165(10)	3.491(14)	1
Mn23	0.6922(5)	1/4	0.5911(13)	3.491(14)	1
O11	0.10374(32)	1/4	0.6455(9)	3.491(14)	1
O12	0.43743(32)	1/4	0.6601(8)	3.491(14)	1
O13	0.76764(35)	1/4	0.6383(9)	3.491(14)	1
O21	0.12017(29)	1/4	0.9952(9)	3.491(14)	1
O22	0.45493(33)	1/4	0.9720(7)	3.491(14)	1
O23	0.80138(35)	1/4	0.9851(7)	3.491(14)	1
O31	0.15268(35)	1/4	0.2360(10)	3.491(14)	1
O32	0.48379(27)	1/4	0.2106(9)	3.491(14)	1
O33	0.83524(34)	1/4	0.1989(8)	3.491(14)	1
O41	0.02365(36)	1/4	0.9107(8)	3.491(14)	1
O42	0.35752(30)	1/4	0.9490(8)	3.491(14)	1
O43	0.70028(38)	1/4	0.9163(8)	3.491(14)	1

[a] Space group: *Pnma*, $a = 26.5058(16)$ Å, $b = 2.83392(13)$ Å, $c = 10.6527(7)$ Å, $z = 12$, Cell volume $= 800.18(8)$ Å^3.

environments of the two manganese sites are comparable. This fact would suggest that Mn^{3+} and Mn^{4+} are likely distributed randomly to a certain degree rather than separated crystallographically.

To check the self-consistency of the structure solutions, the bond valence sum was calculated; +3.78 (Mn1) and +3.65 (Mn2).[26] The estimation is consistent with the rather mixed picture of Mn^{3+} and Mn^{4+}, however, slightly higher than the expected value +3.54. The bond valence sum of the 3*a*-type structure solutions was also calculated: +3.75 (the distortion factor was 19%), +3.93 (17%), +3.75 (16%), +3.34 (16%),

(26) Brown I. D.; Altermatt, D. *Acta Crystallogr.* **1985**, *B41*, 244.

Table 4. Selected Bond Distances in the 3*a*-Type Superstructure of $Li_{0.92}Mn_2O_4$ (HP)

atoms		distances (Å)	atoms		distances (Å)
Mn11	O12 × 2	1.890(10)	Mn21	O11	1.978(17)
	O32	2.086(17)		O22 × 2	2.023(10)
	O41	2.173(16)		O22	2.171(17)
	O41 × 2	1.834(10)		O32 × 2	1.865(9)
Mn12	O11 × 2	2.101(12)	Mn22	O12	2.027(16)
	O33	1.960(15)		O21 × 2	1.969(10)
	O42	1.860(15)		O23	1.960(16)
	O43 × 2	1.792(10)		O31 × 2	1.950(10)
Mn13	O13 × 2	1.858(11)	Mn23	O13	2.062(16)
	O31	1.847(17)		O21	2.118(15)
	O42 × 2	1.981(11)		O23 × 2	1.820(10)
	O43	2.138(16)		O33 × 2	1.963(11)

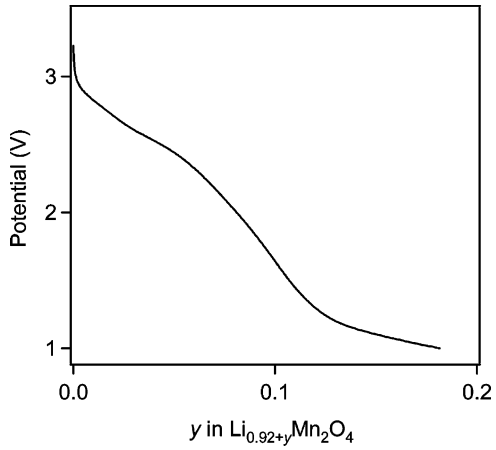

Figure 7. Electrode potential of the $CaFe_2O_4$-type $Li_{0.92+y}Mn_2O_4$ as a function of the amount of intercalated Li ions.

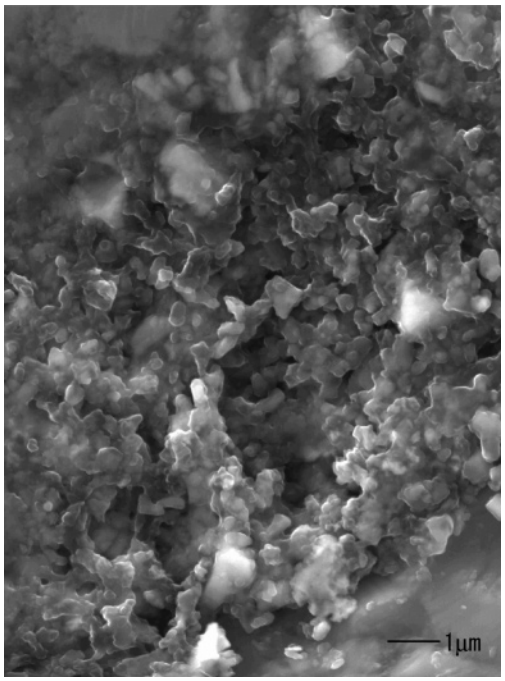

Figure 8. Scanning electron image of the $CaFe_2O_4$-type $Li_{0.92}Mn_2O_4$. Image scale is shown at the bottom.

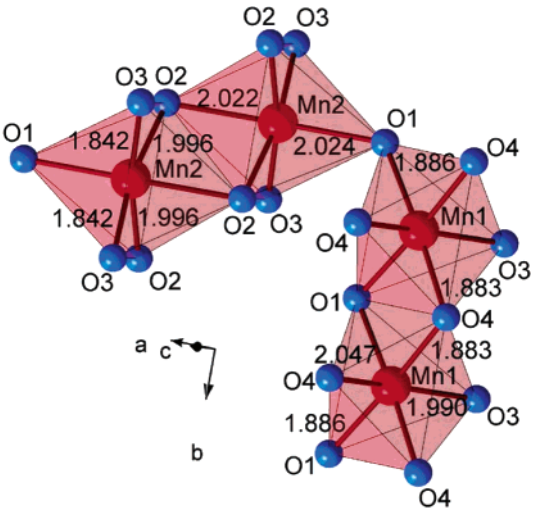

Figure 9. Expanded view of the average structure of the $CaFe_2O_4$-type $Li_{0.92}Mn_2O_4$. The number indicates bond distance (Å). The bond angles are in Table 2.

+3.37 (4%), and +3.64 (16%), for Mn11, Mn12, Mn13, Mn21, Mn22, and Mn23, respectively. The outcome would suggest Mn^{3+} ions are preferred in Mn21 and Mn22 sites. The average of all the sums is +3.63, much better than the result of the average model analysis. However, Mn23−O_6 has a much smaller degree of distortion, while the Jahn−Teller element Mn^{3+} is supposed to be dominant at the site. The fact may suggest that even the large unit cell does not match perfectly with the structure of the compound. Again, we stress that further improvement of sample quality and focused studies on the local structure are needed to make clear the issue. Those are left for future work.

In Figure 10, electrical conductivity data are shown, which were obtained with and without the applied magnetic field of 70 kOe. The temperature vs resistivity plot (inset) clearly shows a semiconducting-like feature. The poor conductivity was found not to recover on cooling to 5 K, and there was very little magnetic field dependence. An Arrhenius plot (main panel) indicates the activation energy (E_h) is 0.27 eV, assuming the hopping conduction picture. The analytic formula employed here was $\sigma = (A/T)\exp(-E_h/k_BT)$, where A is a constant, and k_B is the Boltzmann constant.[27,28] It is nearly two-thirds of that of the spinel ($E_h = 0.40$ eV),[27] suggesting a possible enhancement of hopping mobility due to a certain degree of structure change. Comparison between the two forms of the band structure would be of interest.

Magnetic susceptibility data are shown in Figure 11. The data were measured in the fields of 50 Oe (small panel) and 70 kOe (main panel). In the main panel, a small thermal hysteresis was seen below approximately 10 K, suggesting a magnetically glassy transition as was found in the spinel form.[1−4] A small kink at ~40 K was seen in the weak field ZFC curve (small panel) with a thermal hysteresis, suggesting another magnetic ordering. Alternatively, the impurity Li_2MnO_3 might have a responsibility for the 40 K anomaly because it is antiferromagnetic below 36.5 K.[18]

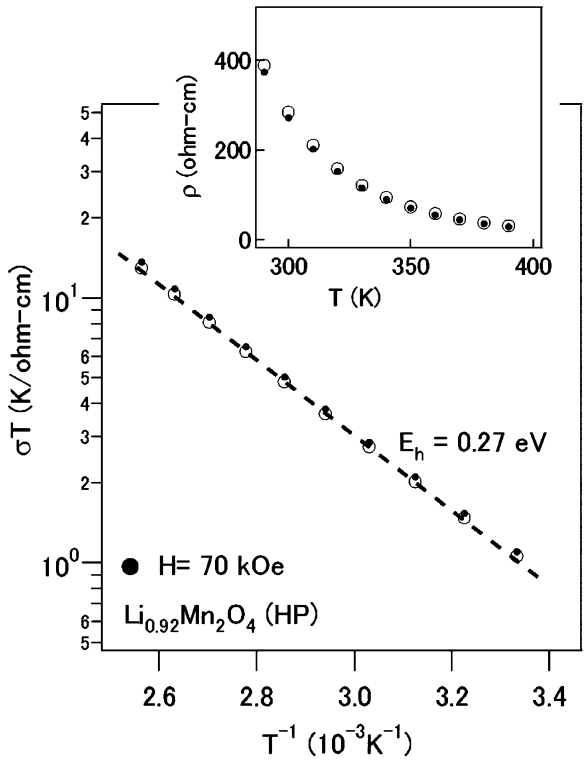

Figure 10. Temperature dependence of the electrical conductivity of the polycrystalline $Li_{0.92}Mn_2O_4$, crystallizing into the $CaFe_2O_4$-type structure (○), and the data measured in the magnetic field 70 kOe (●). The dashed line is a fit to the hopping conduction model.

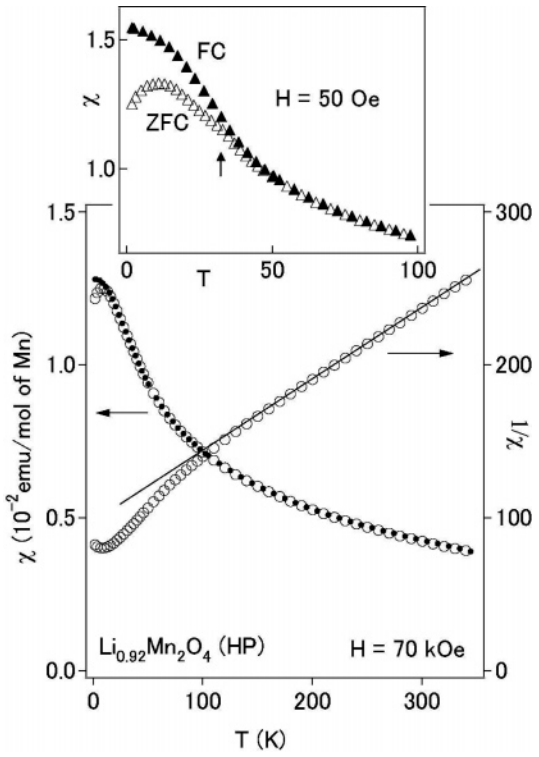

Figure 11. Magnetic susceptibility of the $CaFe_2O_4$-type $Li_{0.92}Mn_2O_4$. Zero-field cooling (ZFC) and field-cooling (FC) data are shown as open and closed symbols, respectively. The data were measured at 70 kOe (main panel) and 50 Oe (top panel). The solid line indicates a Curie−Weiss law fit to the data. The arrow indicates a small kink in the ZFC curve.

In the $1/\chi$ vs T plot of the 70 kOe data, a linear feature appeared, and we applied the Curie−Weiss (CW) law to the

(27) Massarotti, V.; Capsoni, D.; Bini, M.; Chiodelli, G.; Azzoni, C. B.; Mozzati, M. C.; Paleari, A. *J. Solid State Chem.* **1997**, *131*, 94.
(28) Tuller, H. L.; Nowick, A. S. *J. Phys. Chem. Solids* **1977**, *38*, 859.

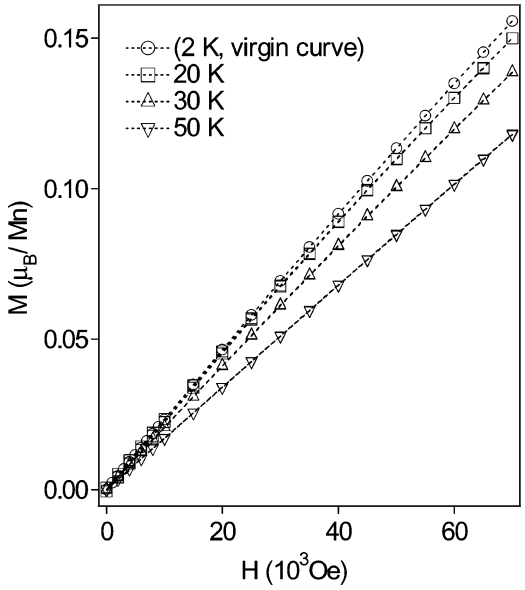

Figure 12. Magnetization curves at various temperatures of the $CaFe_2O_4$-type $Li_{0.92}Mn_2O_4$.

linear part by a least-squares method: $1/\chi(T) = [C/(T - \Theta_W) + \chi_0]^{-1}$, where χ_0 is the temperature-independent susceptibility, C denotes the Curie constant, and Θ_W is the Weiss temperature. The analyzed range was between 150 K and 350 K, and the result is indicated by the solid line. The CW parameters $\mu_{eff} = 3.90(3)\mu_B$, $\theta_W = -180(3)$ K, and $\chi_0 = 2.8(4) \times 10^{-4}$ emu/mol of Mn were obtained. The effective Bohr magneton (μ_{eff}) was calculated from the Curie constant in relation to $C = N_A\mu^2_{eff}/3\pi$, where N_A is Avogadro's constant. The μ_{eff} is rather close to the spin value $3.87\mu_B$ of Mn^{4+} ($S = {}^3/_2$) vs the simple expectation, $4.38\mu_B$, for $Mn^{3.54+}$ (the composition $Li_{0.92}Mn_2O_4$ was assumed), calculated by the formula $\mu_{cal} = \sqrt{(1-x)\mu^2_{S=2}+x\mu^2_{S=3/2}}$, where $\mu_S = 2\sqrt{S(S+1)}\mu_B$ and $x = 0.54$. Perhaps, the coexistence of Mn^{4+} compound Li_2MnO_3 [18] and possible other Mn-rich impurities might be involved somewhat in the origin of the underestimation of μ_{eff}. The Weiss temperature is substantially lower than that of the spinel form ($\theta_W = -266$ K),[29] reflecting the change of the magnetic basis.

Magnetization was measured at 2 K, 20 K, 30 K, and 50 K, and the data are shown in Figure 12. Neither magnetic hysteresis nor spontaneous magnetization was seen in the data at 20 K and above. At 2 K an expected hysteresis from the magnetically glassy transition was found; however the experimental window was too narrow to correctly measure it. We were then able to see only the virgin curve at 2 K. There was no remarkable change in magnetization below and above the magnetic anomaly at ~40 K, which was suggested by the ZFC susceptibility measurement at 50 Oe.

In Figure 13a, specific heat data are shown. A small peak was found at 35 K in both the 70 kOe and the zero-field data. The peak is likely associated with the anomaly found in the weak-field susceptibility data. As the CW analysis to the 70 kOe susceptibility data indicated a substantial antiferromagnetic interaction, the peak is therefore likely due to an antiferromagnetic ordering. To investigate the magnetic contribution further,

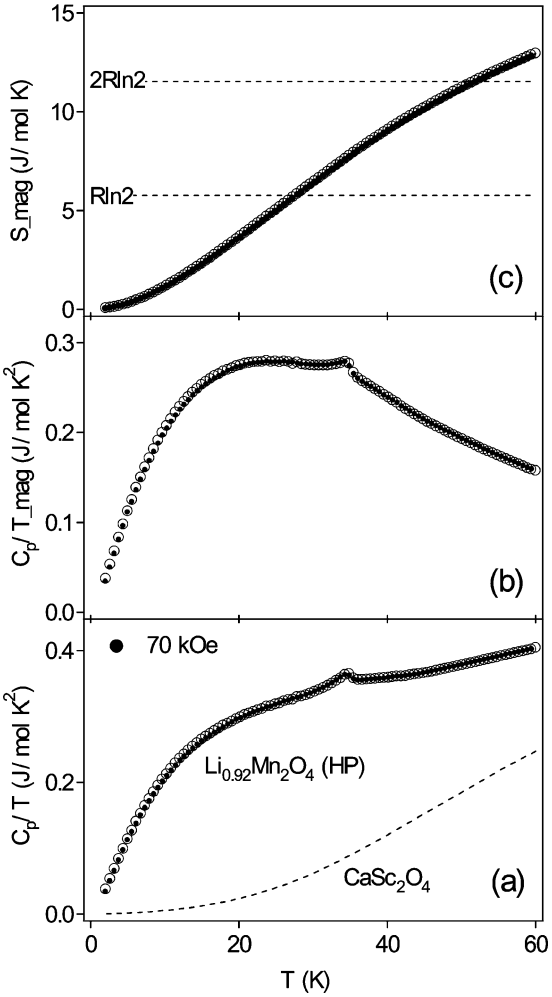

Figure 13. (a) Specific heat of the $CaFe_2O_4$-type $Li_{0.92}Mn_2O_4$ and the isostructural nonmagnetic compound $CaSc_2O_4$, which roughly approximates the lattice contribution. (b) Magnetic part of the specific heat and (c) the magnetic entropy of the $CaFe_2O_4$-type $Li_{0.92}Mn_2O_4$.

the lattice contribution is subtracted from the data in the following way.

The reference material $CaSc_2O_4$ was prepared in the high-pressure furnace from CaO and Sc_2O_3 by heating at 6 GPa and 1300 °C for 1 h.[30] The data for $CaSc_2O_4$ approximates the lattice contribution (dotted curve in Figure 13a), as it is nonmagnetic, isostructural, and has a comparable molecular weight (~7% larger). The magnetic contribution was then separated from the lattice contribution (Figure 13b), and the magnetic entropy was estimated in Figure 13c.

Overviews of the specific heat data are just reminiscent of what were observed for the spinel form, in which a small magnetic peak and substantial magnetic contribution remaining below the peak temperature were found.[2] Due to the broad comparability of the specific heat features (see the small magnetic entropy at the peak and the large entropy loss at low temperature) and the results of the magnetic susceptibility measurements,[1−5] magnetic coexistence of the long-range antiferromagnetic order with the glassy state is likely also in the $CaFe_2O_4$-type form. However, the possibility of the impurity contribution to the small peak (Li_2MnO_3 is antiferromagnetic

(29) Masquelier, C.; Tabuchi, M.; Ado, K.; Kanno, R.; Kobayashi, Y.; Maki, Y.; Nakamura, O.; Goodenough, J. B. *J. Solid State Chem.* **1996**, *123*, 255.

(30) Baranov, M. N.; Kustov, E. F.; Petrov, V. P. *Phys. Status Solidi A* **1974**, *21*, K123.

below 36.5 K[18]) is not excluded. Further studies intended to figure out the magnetic ground state by neutron scattering in addition to the sample quality improvement would be needed.

In summary, we found the spinel-to-$CaFe_2O_4$-type transformation in the lithium manganese oxide, which was induced by heating at 6 GPa. As far as we know there were few studies on the phase transition after the work on the "Spinel" $MgAl_2O_4$ over 15 years ago.[11] It could be interesting to study the transformation further because $LiMn_2O_4$ may share the same structure thermodynamics with $MgAl_2O_4$.

The magnetic susceptibility data and the specific heat data of the $CaFe_2O_4$-type form suggested the magnetically glassy state at low temperature. Further work, including development of sample quality and growth of single crystals, would be advantageous in exploration of possible magnetic anisotropy and in revealing details of the magnetic ground state.

The spinel-type $LiMn_2O_4$ is ideal as a high-capacity battery material because of its low toxicity, low cost, and the high natural abundance of manganese. Recently, much attention has been focused on it and its related compounds to provoke a high electrochemical performance for future rechargeable lithium batteries. The dense version of the compound, reported here, could be significant in deepening the understanding of the nature of the compound and may help to provide valuable opportunities to invent advanced battery technology.

Acknowledgment. This research was supported in part by the Superconducting Materials Research Project from the Ministry of Education, Culture, Sports, Science and Technology of Japan, and by the Grants-in-Aid for Scientific Research from the Japan Society for the Promotion of Science (16076209, 16340111, 18655080), and by the Futaba Electronics Memorial Foundation, Chiba, Japan. We acknowledge the support of the National Institute of Standards and Technology, U.S. Department of Commerce, in providing the neutron research facilities used in this work.

Supporting Information Available: Additional ED patterns and crystallographic information file of the calcium ferrite-type $Li_{0.92}Mn_2O_4$. These materials are available free of charge via the Internet at http://pubs.acs.org.

JA0612302